

1 System Description

Video doorbells provide a set of features common to many traditional video surveillance devices. This distinguishing feature demands a unique power design to ensure trouble-free operation from the ubiquitous, but widely-varying, AC doorbell supply. To fully utilize an AC source that presents a substantial bottleneck, the power design should be as efficient as possible. This design uses TI's new synchronous buck converters and LDOs providing a complete and customizable supply optimized for video doorbells. Our newest converters in QFN and SOT-563 packages allow for a supply design that requires minimal board space and has a low thermal impact—both of which are needed for smaller form factor electronics. For better compatibility, sequencing is possible for all rails.

IP network cameras have increasing image resolution, processing, and illumination requirements while still fitting in small enclosures. After stepping down from a mid- to high-voltage DC power source such as plug-in power or PoE, the system demands point-of-load conversion with high efficiency and a small footprint. Both efficiency and footprint are important to accommodate small enclosures with, typically, less-than-adequate ventilation. This design is optimized for both efficiency and footprint while also providing the flexibility to tailor to more advanced, power-demanding loads, such as a dedicated image recognition processor or 4K video processor.

Wireless or battery-powered cameras require high efficiency at both full loads and light loads. These cameras typically employ motion detection, human interface, or wireless communications monitoring, or any combination of the three, to minimize time spent in power-hungry states quiescent currents and shutdown currents of subsystems are very important as these standby currents can have significant impact on overall battery life. The TIDA-01579 reference design has been optimized for this application by utilizing TI's low-power converters featuring both light load efficiency and shutdown with low I_q . Converter shutdown and low- I_q load switches can be used to cut power to subsystems with less-than-desirable standby consumption—saving cost and extending battery life.

2 System Overview

2.1 Block Diagram

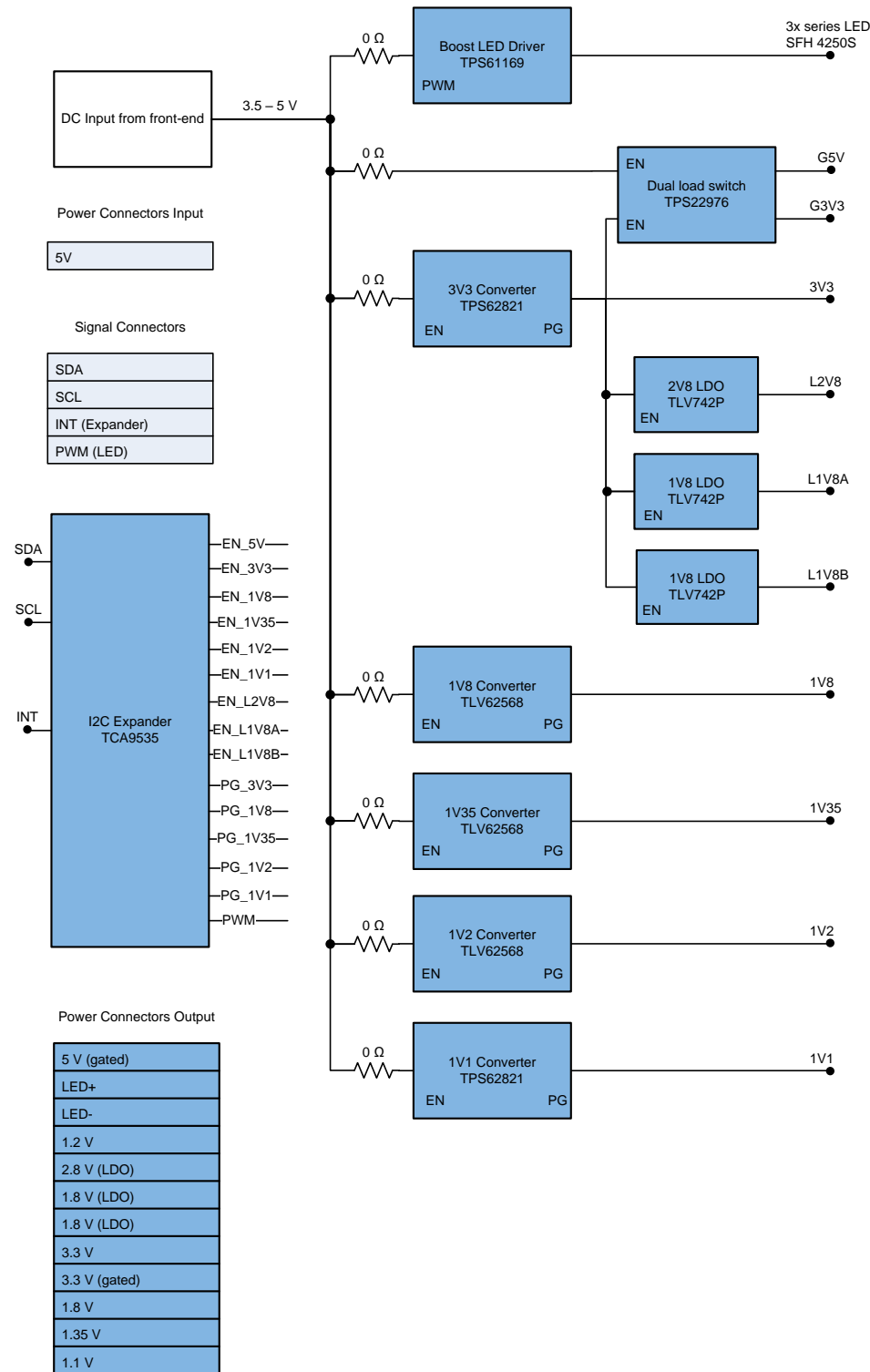


图 1. Block Diagram

3 Highlighted Products

With small footprint, and high efficiency DC/DC regulators from TI, it is possible to design compact, highly-efficient point of load power solutions.

3.1 TLV62568

The TLV62568 device is a synchronous step-down buck DC/DC converter optimized for high efficiency and compact solution size. The device integrates switches capable of delivering an output current up to 1 A. At medium to heavy loads, the device operates in pulse width modulation (PWM) mode with 1.5-MHz switching frequency. At light load, the device automatically enters power save mode (PSM) to maintain high efficiency over the entire load current range. In shutdown, the current consumption is reduced to less than 2 μ A. The device is available in a SOT23 and SOT563 package

3.2 TPS62821

The TPS6282x is an all-purpose and easy-to-use synchronous step-down DC/DC converter with a very-low quiescent current of only 4 μ A. It supplies up to 3-A output current (TPS62823) from a 2.4-V to 5.5-V input voltage. Based on the DCS-Control™ topology it provides a fast transient response.

The internal reference allows regulating the output voltage down to 0.6 V with a high feedback voltage accuracy of 1% over the junction temperature range of -40°C to 125°C . The TPS6282x are packaged in a 2-mm \times 1.5-mm QFN-8 package.

3.3 TLV742P

The TLV742P series of low-dropout (LDO) linear voltage regulators are optimized to providing excellent performance by supporting a wide output voltage range. The LDO regulators can directly regulate a single cell Li-ion battery input-to-output voltage as low as 0.85 V. If used to post-regulate a DC/DC converter output, the high PSRR of 55 dB at 1 MHz suppresses ripple to provide a stable low-noise, well-regulated output voltage. The TLV742P series of voltage regulators are available in a 1-mm \times 1-mm X2SON package to minimize the PCB area.

3.4 TCA9535

The TCA9535 is a 24-pin device that provides 16 bits of general purpose parallel input and output (I/O) expansion for the two-line bidirectional I²C bus or (SMBus) protocol. The device can operate with a power supply voltage ranging from 1.65 V to 5.5 V. The TCA9535 device consists of two 8-bit configuration (input or output selection), input port, output port, and polarity inversion (active-high or active-low operation) registers.

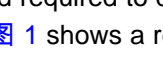
3.5 TPS61169

With a 40-V rated integrated switch FET, the TPS61169 is a boost converter that drives LEDs in series. The boost converter has a 40-V, 1.8-A internal MOSFET with minimum 1.2-A current limit; thus it can drive single or parallel LED strings for small- to large-size panel backlighting. The TPS61169 device is available in a space-saving 5-pin SC70 package.

3.6 TPS22976

The TPS22976 product family consists of two devices: TPS22976 and TPS22976N. Each device is a dual-channel load switch with controlled turn on. The device contains two N-channel MOSFETs that can operate over an input voltage range of 0.6 V to 5.7 V, and can support a maximum continuous current of 6 A per channel. Each switch is independently controlled by an on and off input (ON1 and ON2), which can interface directly with low-voltage control signals. The TPS22976 device is capable of thermal shutdown when the junction temperature is above the threshold, turning the switch off. The switch turns on again when the junction temperature stabilizes to a safe range. The TPS22976 device also offers an optional integrated 230- Ω on-chip load resistor for quick output discharge when the switch is turned off. The TPS22976 is available in a small, space-saving 3-mm \times 2-mm 14-SON package (DPU) with integrated thermal pad allowing for high power dissipation.

4 System Design Theory

Video surveillance products such as a video doorbell or Wi-Fi® camera typically consist of power processor interfacing with high-speed image sensor and video encoder. The processor also interfaces with SD ram, audio codec supporting two-way audio communication, lens driver with IR cut filter sub circuitry. From power perspective many different supply rails are needed to be generated required to drive core voltage, I/O rail, and analog voltage for the previously-mentioned peripherals.  shows a representation of typical power tree.

4.1 Buck DC/DC Regulator

For this application as fast transient response, low voltage ripple in a small form factor is required, selecting right control topology is the first step. Buck Converter has two sections that impact the performance, one is the power stage and other is the control topology. Power stage remains the same for all control topology. The inductor value is computed based on the preferred mode of switching operation. Whereas the control loop effects the loop response time, switching frequency, voltage ripple, full and light load efficiency.

The TI portfolio offers devices with 12 different types of control architectures. Most-commonly used are output voltage control, peak current control, hysteretic or adaptive or fixed on time. Application requirements are driving factors for selecting the control topology. In this application a fast output response is needed, low voltage ripple, high DC voltage accuracy with minimum external components and seamless transition from PWM to power save mode, DCS-Control architecture is selected for high current demanding rail such as MPU Core voltage. This architecture offers benefits of both Voltage control loop for high DC accuracy and hysteretic control loop for seamless transition, fast response with minimum external components with only trade off of wide variation of switching frequency as function of load current. Post damped PI filters have been implemented to counter impact of wide switching frequency ripple voltage variation on peripheral supply rail.

4.1.1 Power Stage Design Consideration

Before computing the Power stage Inductor & Capacitor values, the operating mode for maximum period of operation is considered. For rails that operate most of time in moderate to full load CCM mode is considered (Core Voltage and 3.3 V) whereas for rails which operate most of time in light to moderate load DCM mode is considered (DDR3 and Sensor Voltage).

4.1.1.1 Inductor Ripple Current CCM Mode

In CCM mode the inductor ripple is a non-zero AC triangular ripple waveform with DC offset equal to output current as 图 2 shows.

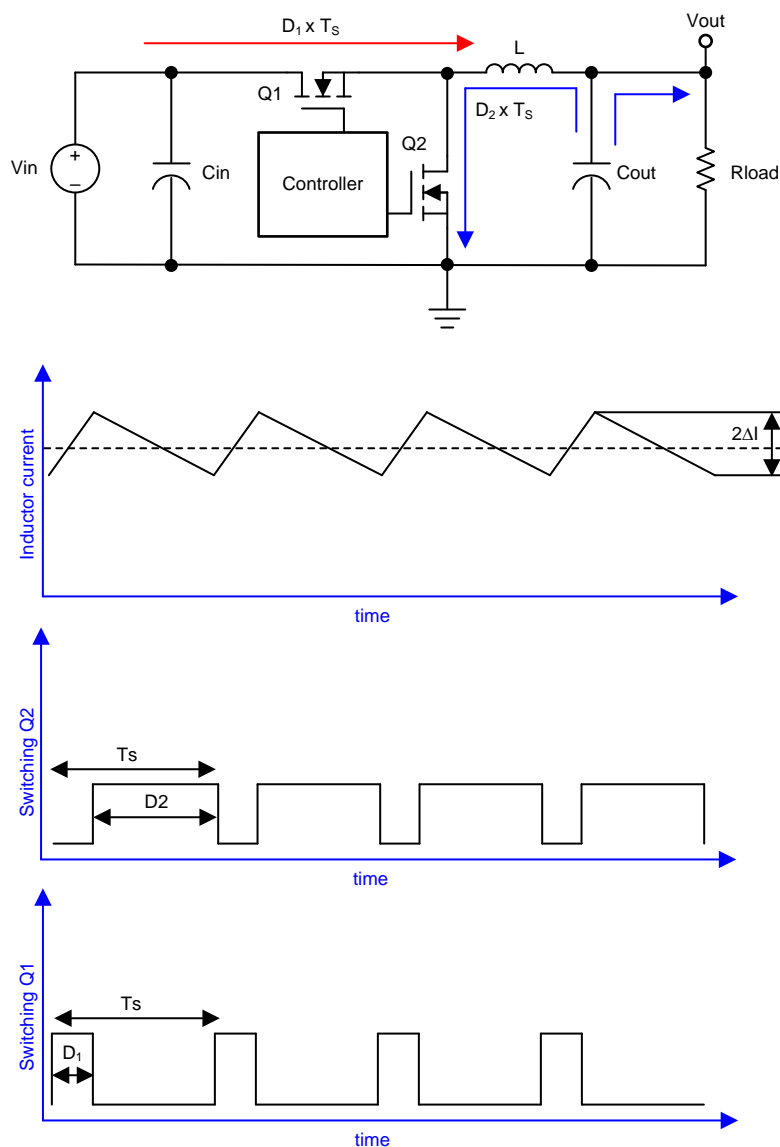


图 2. CCM Mode Operation

CCM Mode reduces AC core loss in inductor for moderate to full load. For making the flux swing in inductor core less than one half of maximum flux density, ripple current should be kept between 20%–40% of output DC current. In CCM mode there are two paths in one switching cycle. To reduce DC loss and reduce thermal hotspot for full load current, it is required that the DCR of inductor be as low as possible. To achieve very small DCR, lower no of turns is required which will result into smaller inductance value. Smaller inductor will result into higher ripple current dominating core and AC losses. Inductor has been selected keeping into consideration of both AC and DC losses in this design.

Compute the operating duty cycle and power stage inductor using 公式 1 and 公式 2:

$$D = \frac{V_{out}}{V_{in}} \quad (1)$$

$$L = \frac{(V_{in} - V_{out}) \times D}{(0.2 \text{ to } 0.4) \times I_{outmax} \times f_{sw}} \quad (2)$$

4.1.1.2 Inductor Ripple Current DCM Mode

In DCM mode, the inductor ripple is an AC triangular ripple waveform with zero crossing in each switching period as [图 3](#) shows.

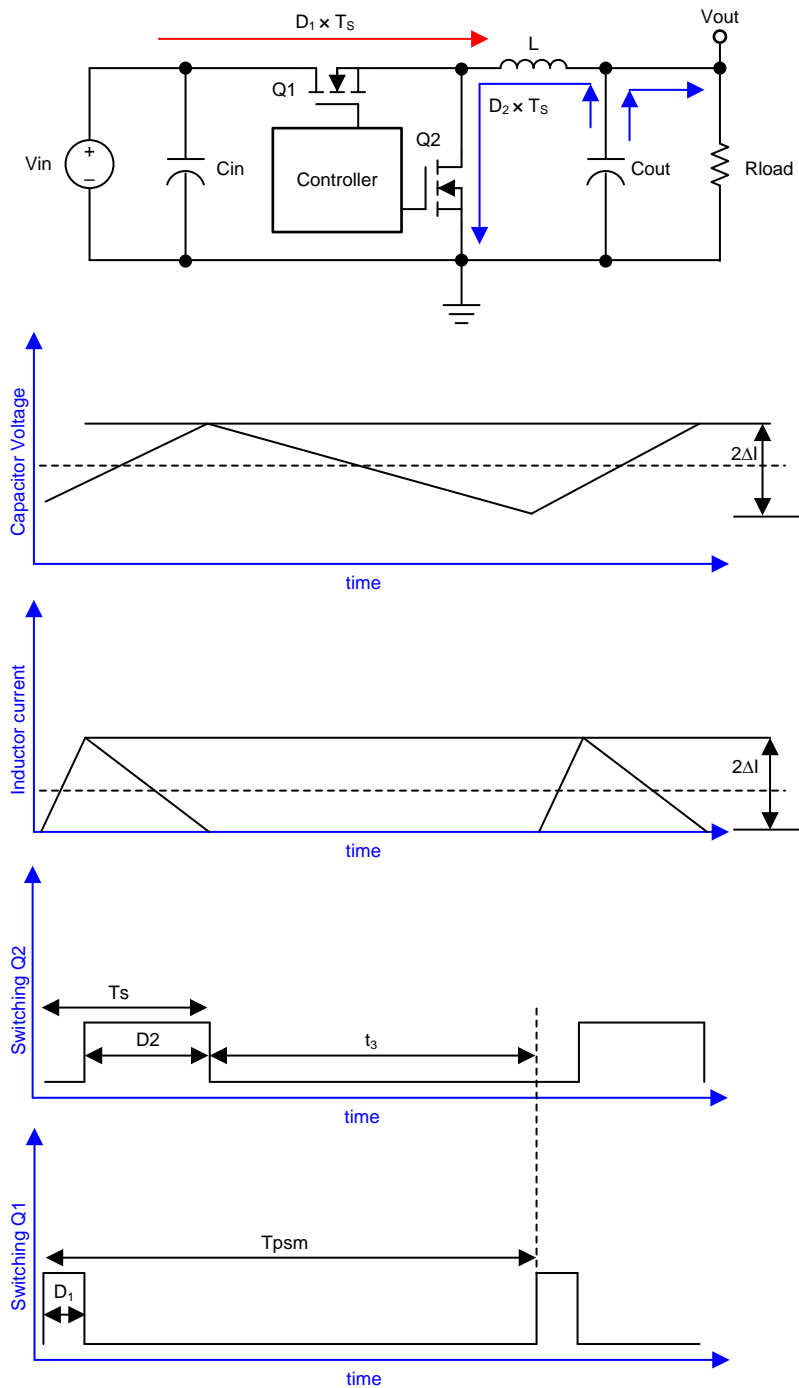


图 3. DCM Mode Operation

At light loads the ensure the flux swing in the inductor core still remains less than one half of maximum flux density. Using average equation of triangular waveform ($1/2 \times \text{base} \times \text{height}$) the ripple current needs to higher than twice of output current for one switching period as shown if fig. For ratio greater than 2 the inductance size can be further brought down thus increasing ripple current. In such scenarios the pause time t_3 increases thus decreasing output voltage ripple frequency.

In this mode there are three states in one switching cycle described as on time (D1TS), off time (D2TS) and pause time (t_3). Pause time is function of output load current and output capacitor value. At load conditions that satisfy condition as shown in equation 公式 3 results into DCM mode operation.

$$L < \frac{R_L}{2 \times f_{sw}} \quad (3)$$

4.1.1.3 Output Capacitor

An output capacitor with a power inductor forms the second-order low-pass filer attenuating the switching ripple voltage and also as energy storage for fast transient loads above a closed-loop bandwidth. At a higher switching frequency, the capacitance lead inductance also comes into the picture which is known as ESL and ESR of the capacitor as 图 4 shows.

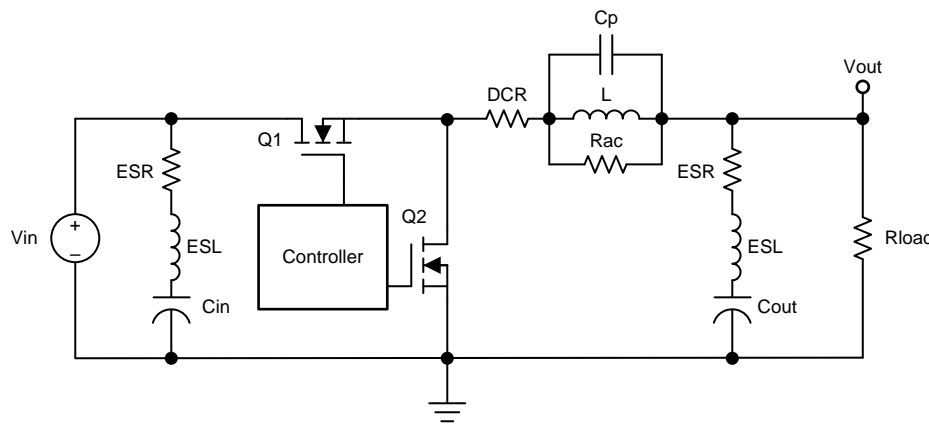


图 4. Non-Ideal Buck Converter

The expected ripple voltage in the CCM mode output capacitor can be computed using 公式 4. A capacitor with low ESR and low ESL reduces the output ripple voltage. For ESL values of picohenrys, the ESL factor can be ignored:

$$C_{out} = \frac{1}{8 \times f_{sw} \left(\frac{\Delta V - (ESL \times \frac{V_{in} - V_{out}}{L})}{di} \right) - ESR} \quad (4)$$

In the case of DCM mode output, ripple voltage will be slightly higher based on pause time and output current which retriggers internal comparator of DC/DC converter when ripple voltage is lower than threshold. To derive output voltage ripple we can integrate capacitor current as shown in waveform during turn on and take twice of its value to get peak to peak ripple voltage. Capacitor current during turn on pulse can be put together as 公式 5 shows:

$$I_C = \frac{(V_{in} - V_{out}) \times t_{on}}{L} - I_{out} \quad (5)$$

Solving the integration during the turn on period for capacitor current and capacitor voltage is expressed as 公式 6 shows:

4.1.4 PI Filter

Switching regulators generates undesired output artifacts that are harmful to noise critical rails. LDO do offer best rejection for post filtering but result into higher thermal losses at high load currents. An effective method to filter high frequency components is to use ferrite bead in PI configuration with capacitor to introduce low pass filter. 图 5 shows most common filtering scheme implemented in power circuits.

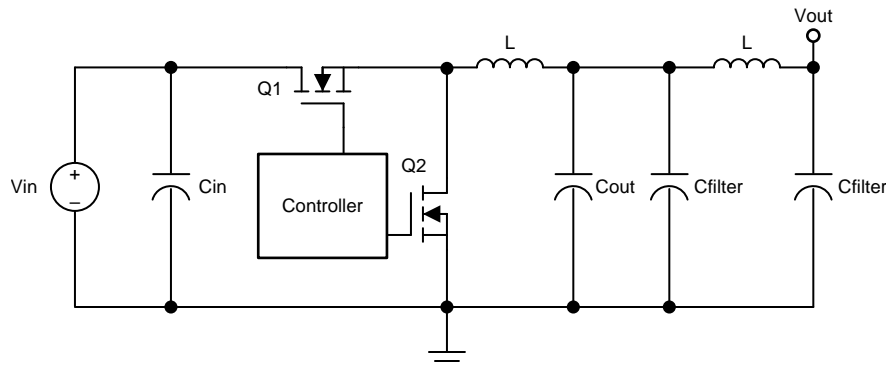


图 5. PI Filter

Ferrite bead detailed equivalent circuit analysis is considered to understand effects of self-resonance and LC resonance on gain plot to design effective filtering network. Ferrite bead has three operation regions: inductive, resistive and capacitive. These regions can be located from ZXR plot of ferrite bead as shown in 图 6. The Ferrite bead can be modeled using an inductor, capacitor and resistor as 图 6 shows, were RDC is DC resistance; Cpar, Lpar and Rac are bead inductance, capacitance and AC core loss resistance

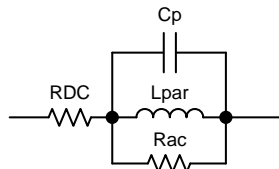


图 6. Bead Equivalent Model

Using an impedance curve for zero DC bias above values can be computed as per 公式 9, 公式 10, and 公式 11.

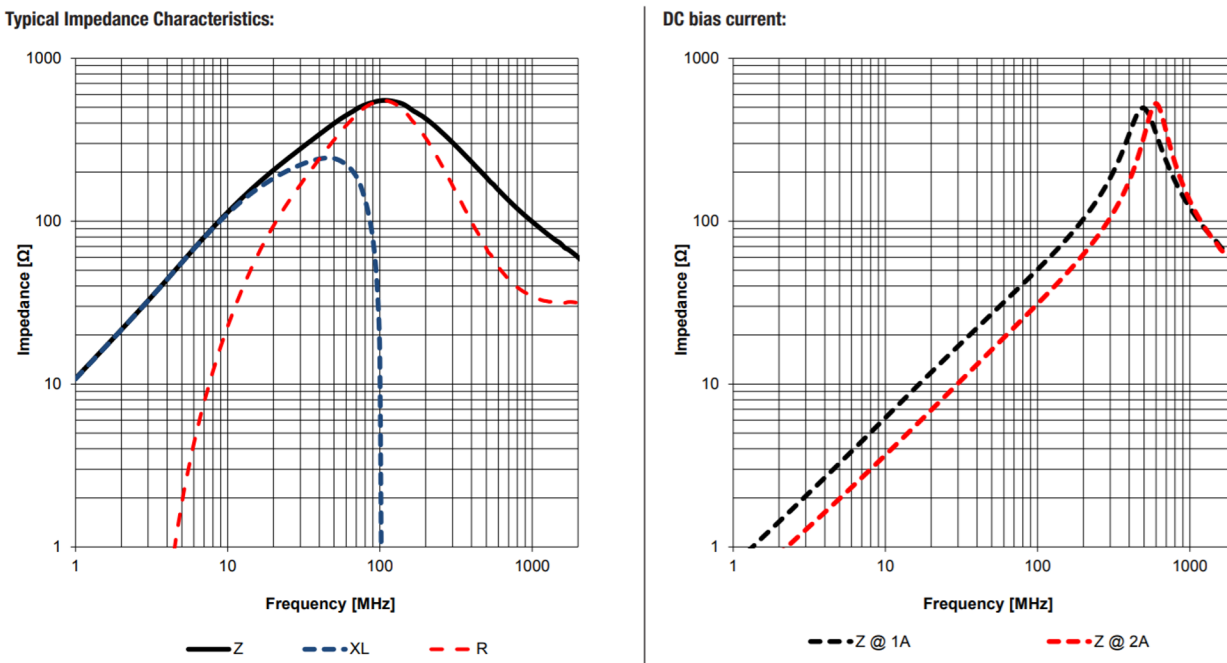


图 7. Impedance Curve

$$L_{\text{par}} = \frac{Z_L}{2 \times \pi \times f_L} \quad (9)$$

$$C_{\text{par}} = \frac{1}{2 \times \pi \times Z_C \times f_C} \quad (10)$$

$$R_{\text{AC}} = Z_{\text{resonance}} = \frac{1}{2 \times \pi \times C_{\text{par}} \times f_{\text{resonance}}} = 2 \times \pi \times L_{\text{par}} \times f_{\text{resonance}} \quad (11)$$

The data sheet also gives characteristics curve of impedance vs frequency for various DC Bias current.

For maximum output current there will be shift in DC Inductance which needs to be calculated as it impacts into shift of corner frequency towards right side.

Assuming a ripple voltage of 25 mV at 2.2 MHz and required ripple voltage of 25 µV the required attenuation is -54 dB. Using ideal LC second order equation, resonant frequency of LC and filter capacitor can be calculated using 公式 12 and 公式 13.

$$f_{LC} = \frac{f_a(2.2 \text{ MHz})}{\sqrt{\left(\frac{1}{10}\right)^2 - 1}} \quad (12)$$

$$C_{\text{filter}} = \frac{1}{2(4 \times \pi^2 \times f_{LC}^2 \times L_{\text{par}})} \quad (13)$$

A ferrite bead with a self-resonant frequency of at least 20, to approximately 50 times greater than switching frequency needs to be selected to operate in inductive region. Using a true bead model with output decoupling capacitor we see peaking occurring which results in gain at resonant frequency component as shown in 图 8.

So LC filter needs to damped to reduce the peaking. Using series resistor damping can be achieved but will result into increased DC loss and voltage drop, Adding damp resistor in parallel to ferrite bead is another technique but results in bypass path at higher switching frequency.

One of the best techniques to avoid issue is to add bulk capacitor with series resistor which not only damps the peak but also does not degrade the effectiveness of filtering. Damp capacitor needs to higher than DC/DC output capacitor, at least 5 times will reduce value of series damp resistor.

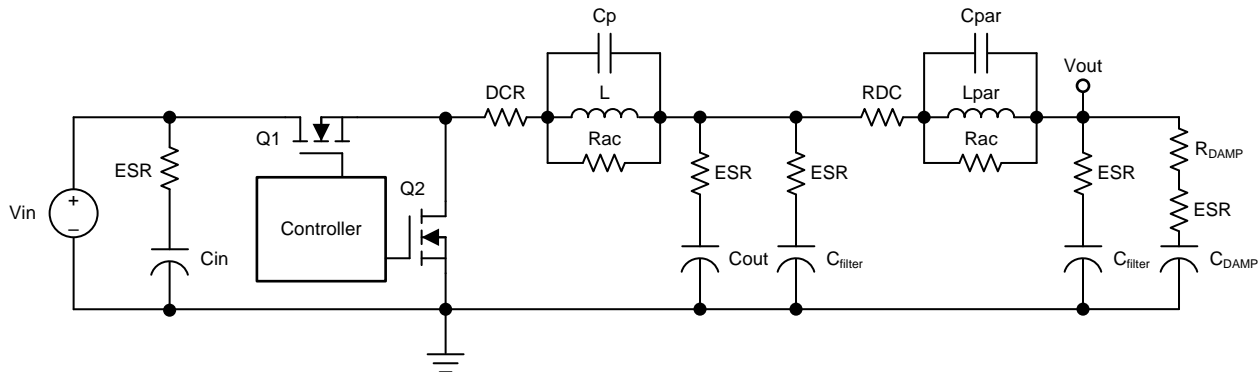


图 8. Non-Ideal PI Filter

Using 公式 14 damp resistor can be computed.

$$R_{damp} \leq 0.5 \times \sqrt{\frac{L_{par}}{C_{filter}}} \quad (14)$$

Comparing simulation data as shown in 图 9 and 图 10 for damping circuit we see attenuation for desired frequency region with damping of LC resonance.

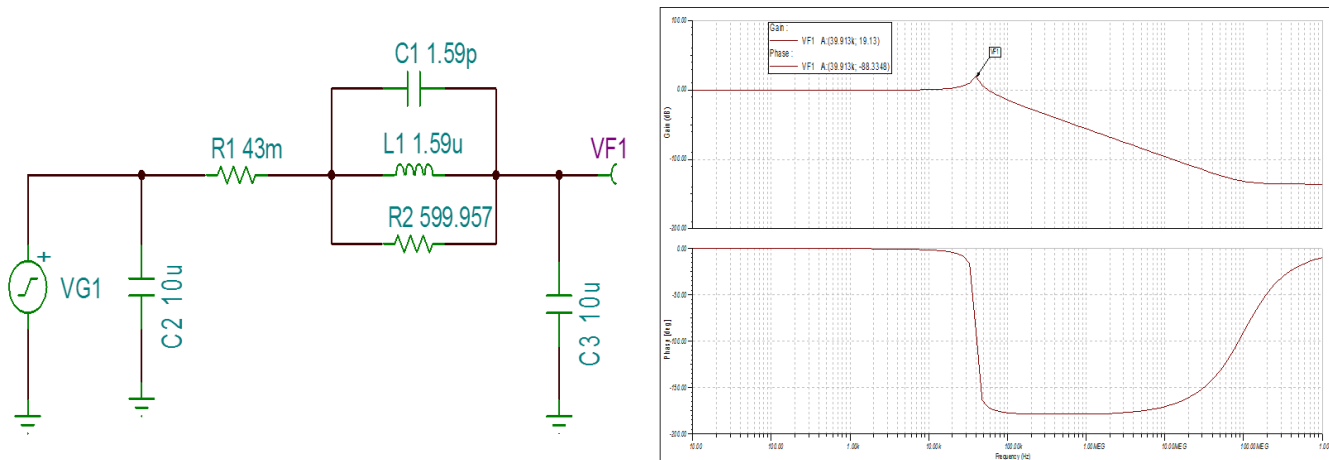


图 9. Undamped Filter Response

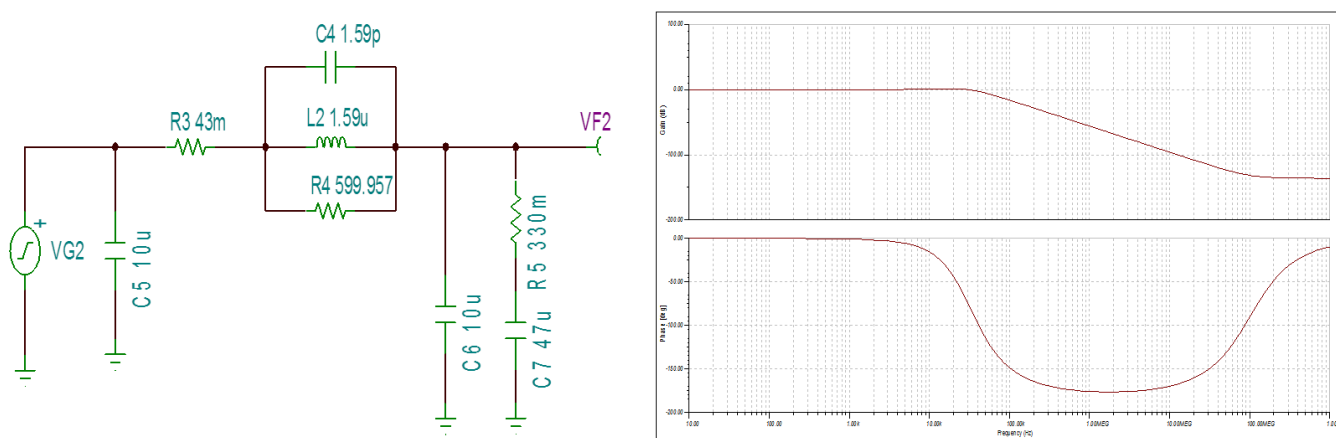


图 10. Damped Filter Response

4.1.5 Boost LED Driver

TIDA-01579 board has provision of Boost LED Driver to test IR LED illumination typically required in Video Imaging application. For more details refer to the [TIDA-01586](#) design.

4.2 PCB Layout Consideration

PCB Layout determines Ground bounce, Electromagnetic Interference (EMI), and Thermal Behavior of switching regulator circuit. In switching regulator circuits there are fast switching node currents due to operation of synchronous FET. This gives rise to fast dI/dt currents.

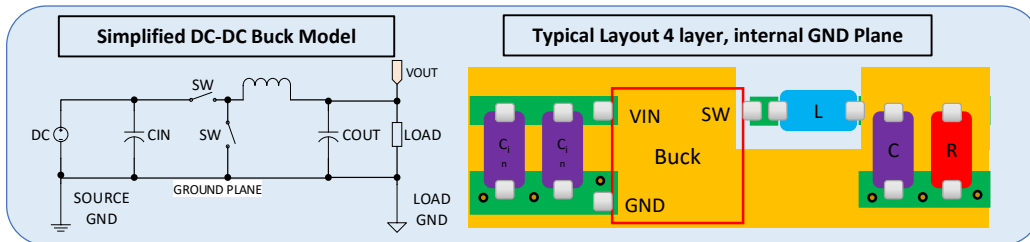


图 11. Typical Buck Converter Layout

Switching current flowing through return trace will result into change of flux which is function of loop area and magnetic flux density linked to it. In case of poor layout techniques having large ground loop, the fast switching current will results in rise of transient voltage, EMI interference and changing potential between actual ground and load ground. This impacts accuracy of output voltage.

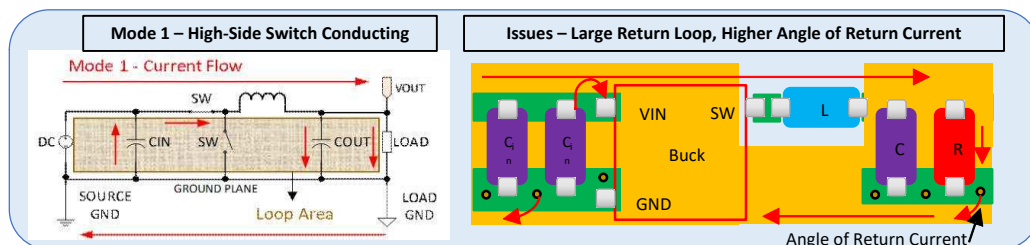


图 12. Mode 1 Switching Current

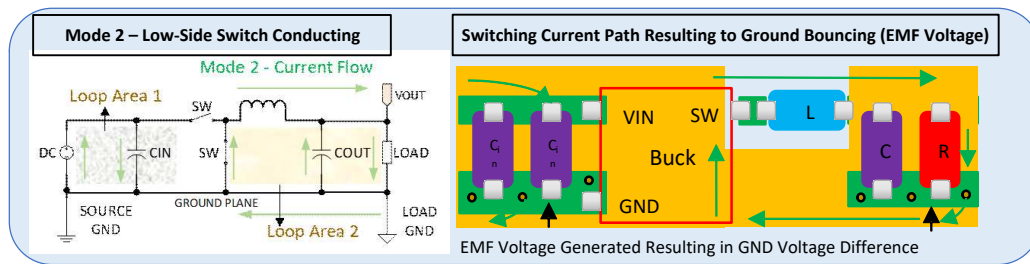


图 13. Mode 2 Switching Current

Placement of input capacitor, output capacitor, and power inductor with respect to switching point of device determines loop area of switching node. Adding even ground plane in inner layer does not minimize ground bounce issue.

To mitigate the previously-discussed issues, ground loop between switching node needs to be minimized. The placement of input and output capacitors must have a very short return ground plane as 图 14 shows. To avoid operating issues due to PCB layout errors, see the *TI Layout* guidelines mentioned in the data sheet.

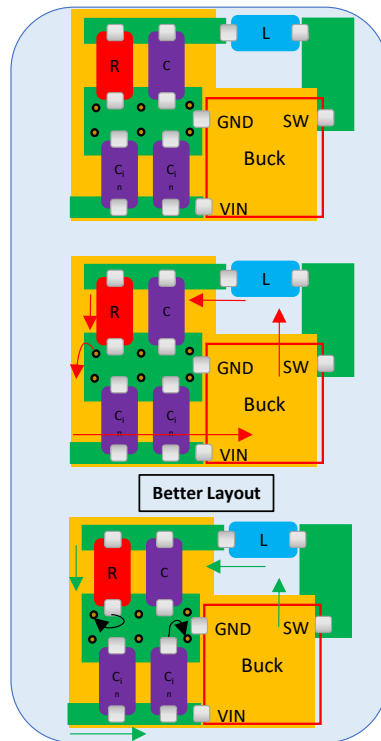


图 14. Recommended Layout

For example, in the layout for IC, U3 the input capacitor C25, output capacitor C26, power inductor L6 and are placed with lowest return path.

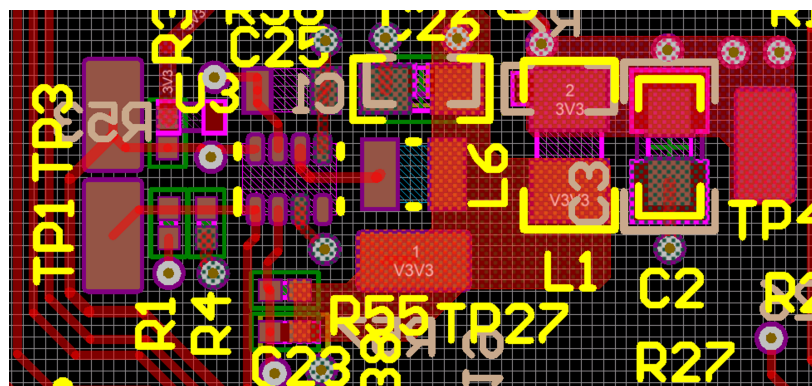
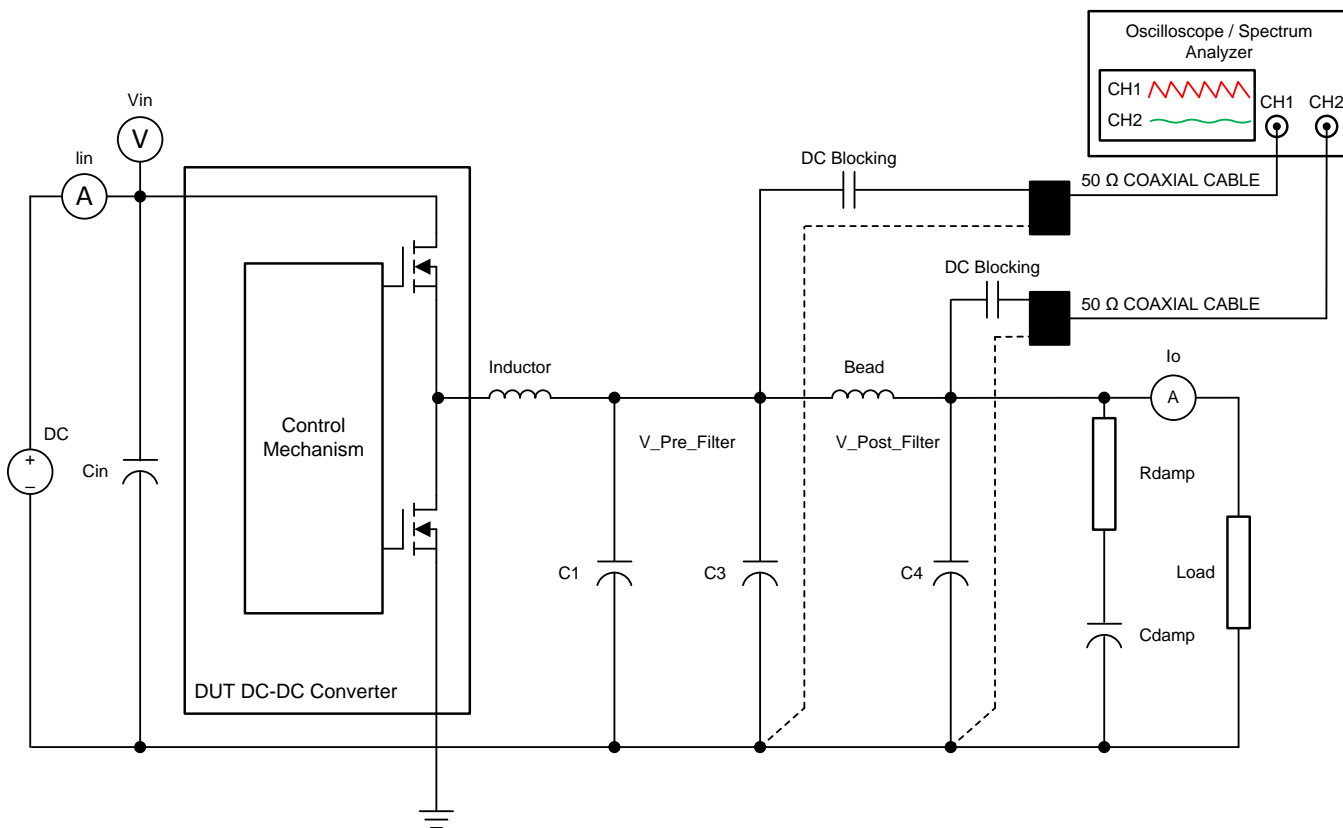


图 15. DC/DC Layout Example

6 Test Setup

The test setup consists of TIDA-00753 Board, Keithley DC Supply, Agilent DMM, Decade Box, Current Probe as [图 16](#) shows.



DUT: device under test

The oscilloscope analog signal bandwidth must be greater than 400 times the switching frequency

The oscilloscope should have a higher memory depth and sampling rate to capture the ripple waveform accurately (at least 4 GSPS, memory depth > 1 Mpts)

Oscilloscope probe terminated to 50 Ω

Set the spectrum analyzer with a frequency resolution less than 100 times the switching frequency to capture a better noise floor and SPUR

图 16. TIDA-01579 Test Setup

The tests to be conducted for this design are:

1. Device Efficiency and System Efficiency at various load and input voltage range
2. Ripple Voltage, Ripple Frequency at Full and light load conditions, Output Voltage Accuracy, Standard Deviation, Min and Max for various light and full load current's
3. Line and Load Transient Response
4. Light and Full Load Thermal Capture

To test the previous condition, the Agilent 61/2 DMM is set with the following settings to average the source and instrument error

1. Slow Filter – 7 seconds/ Reading
2. No of Samples – 50 (Approximately 6 min)

7.2 Point of Load Pre and Post Output Voltage Ripple and FFT Plots

Using the *Spectrum Analyzer* function, 1x AC probe as shown in the Test Setup Image, Spectrum plot have been captured for all DC/DC rail to validate very low ripple output and Harmonic free Spectrum to achieve Higher ENOB with respect to Power supply Spur and Noise Floor.

7.2.1 3.3-V Output

表 12. 3.3-V Ripple and FFT Plot

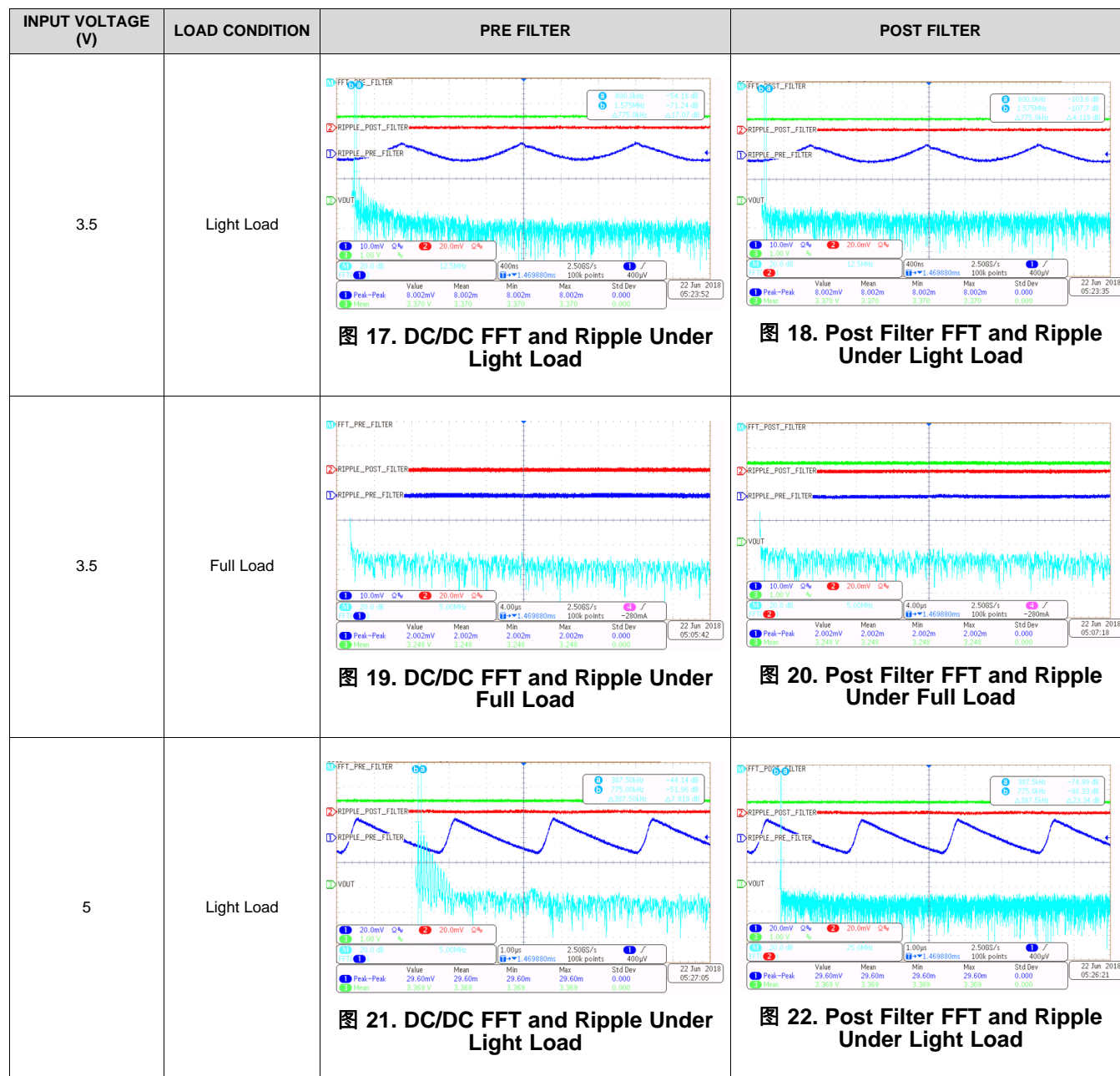
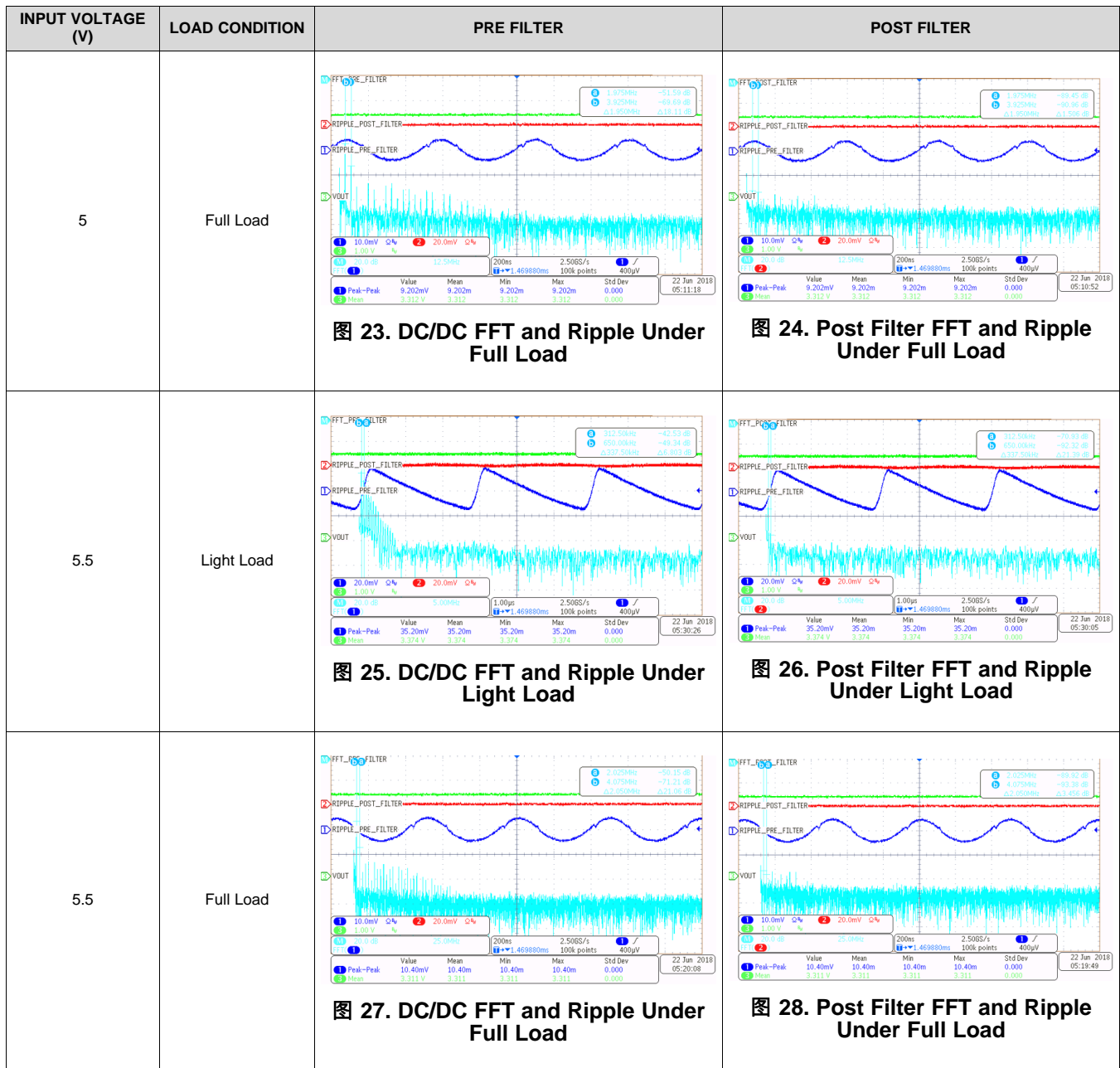


表 12. 3.3-V Ripple and FFT Plot (continued)



7.2.2 1.1-V Output

表 13. 1.1-V Ripple and FFT Plot

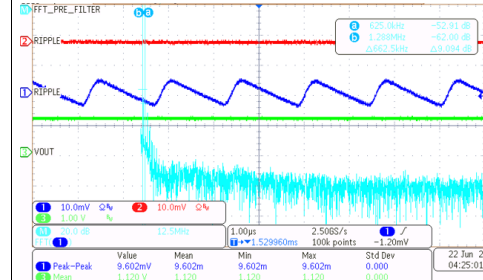
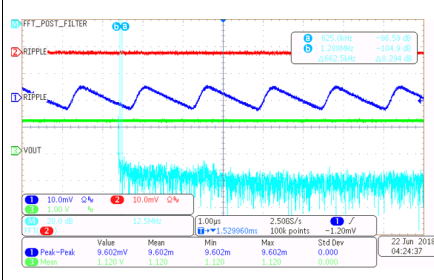
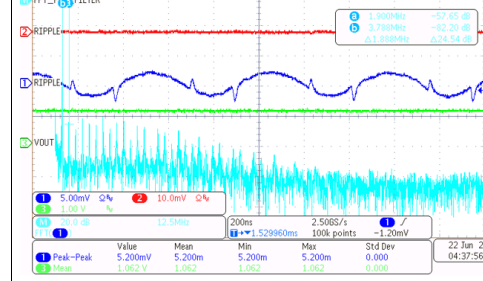
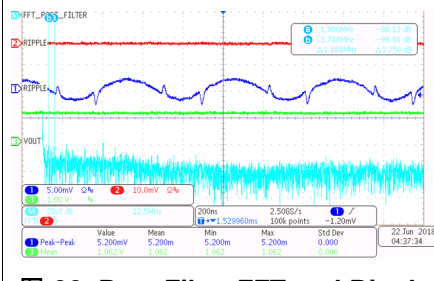
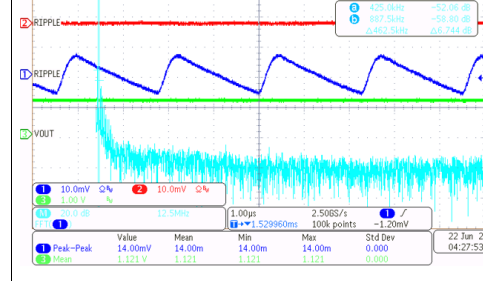
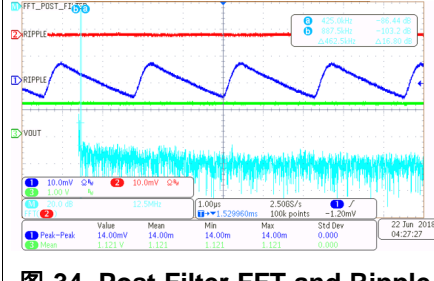
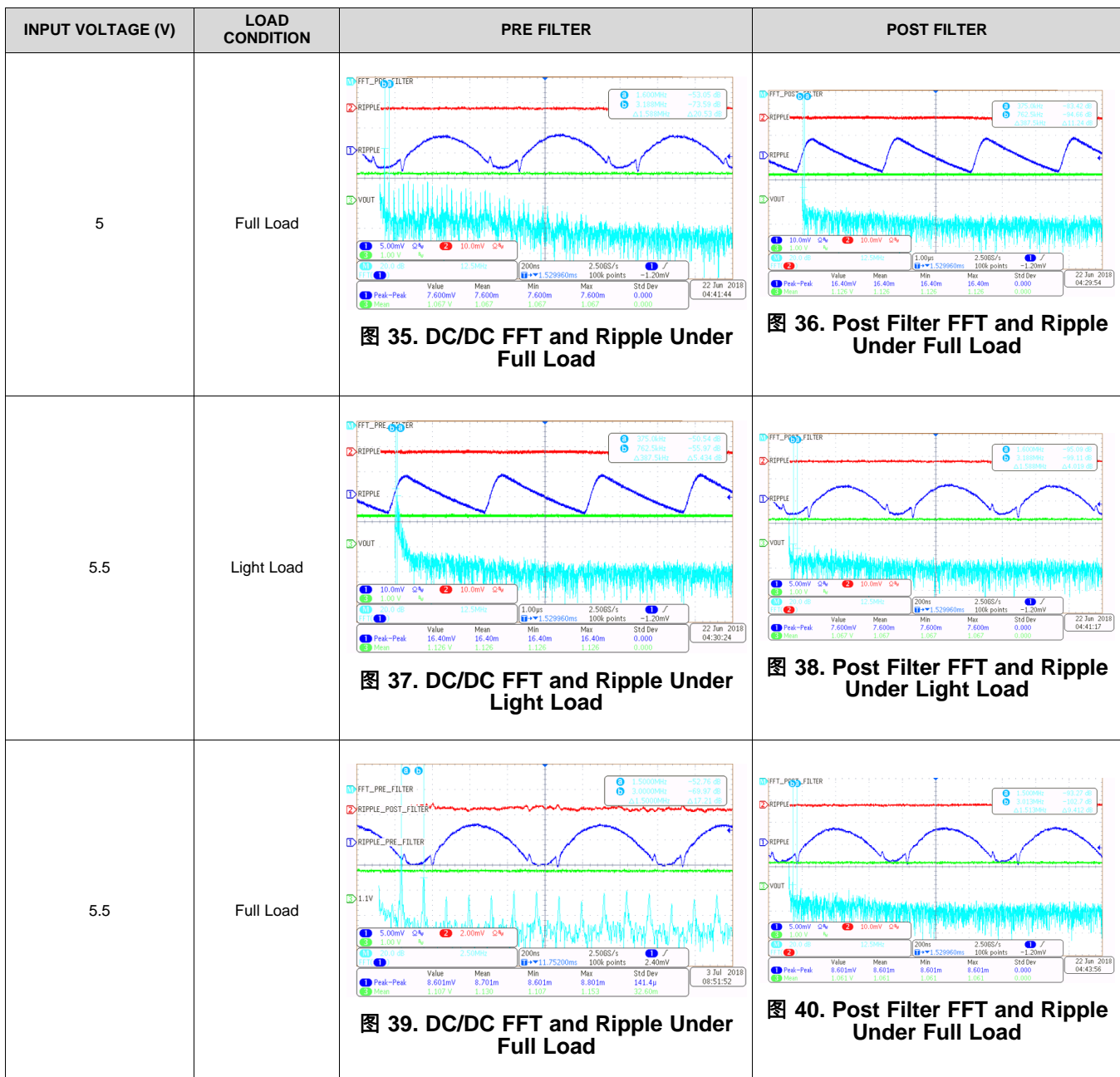
| INPUT VOLTAGE (V) | LOAD CONDITION | PRE FILTER | POST FILTER |
|-------------------|----------------|--|---|
| 3.5 | Light Load |  <p>图 29. DC/DC FFT and Ripple Under Light Load</p> |  <p>图 30. Post Filter FFT and Ripple Under Light Load</p> |
| 3.5 | Full Load |  <p>图 31. DC/DC FFT and Ripple Under Full Load</p> |  <p>图 32. Post Filter FFT and Ripple Under Full Load</p> |
| 5 | Light Load |  <p>图 33. DC/DC FFT and Ripple Under Light Load</p> |  <p>图 34. Post Filter FFT and Ripple Under Light Load</p> |

表 13. 1.1-V Ripple and FFT Plot (continued)



7.2.3 1.35-V Output

表 14. 1.35-V Ripple and FFT Plot

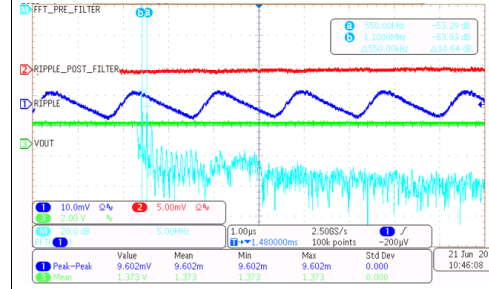
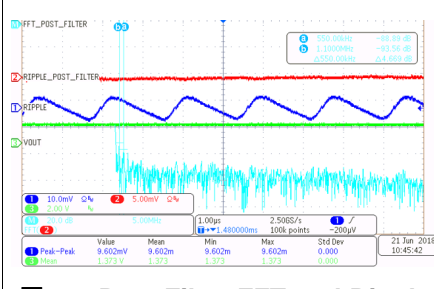
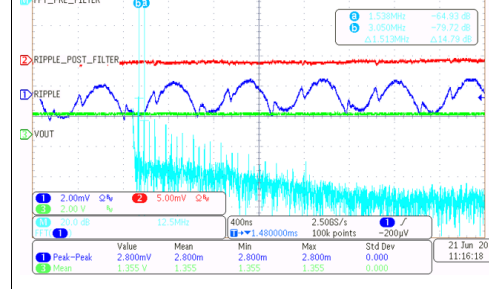
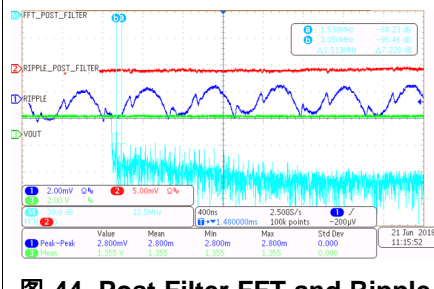
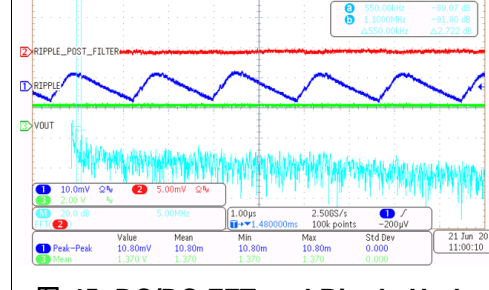
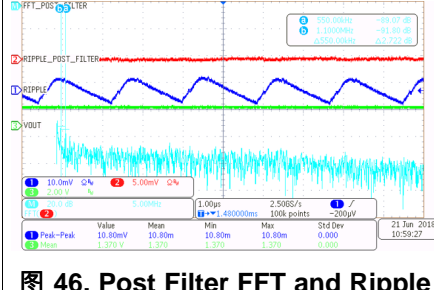
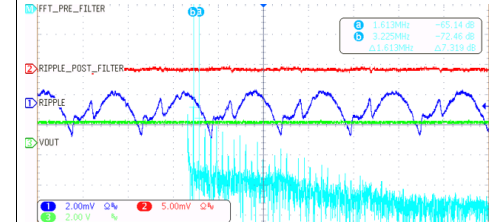
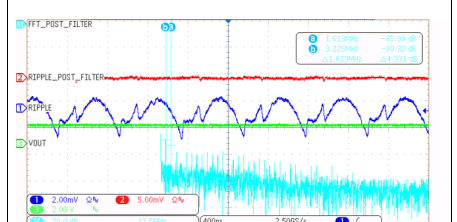
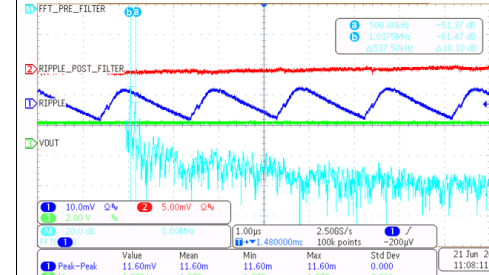
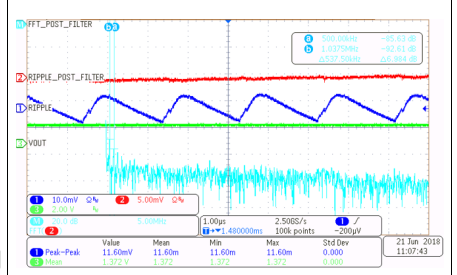
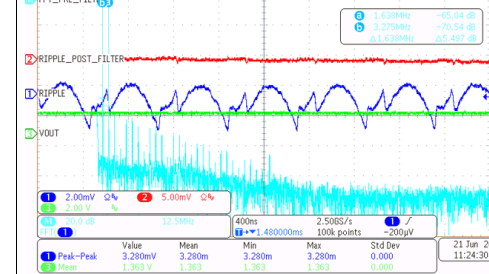
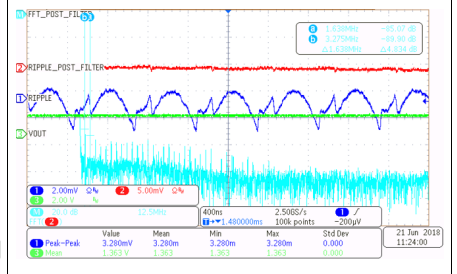
| INPUT VOLTAGE (V) | LOAD CONDITION | PRE FILTER | POST FILTER |
|-------------------|----------------|--|---|
| 3.5 | Light Load |  <p>图 41. DC/DC FFT and Ripple Under Light Load</p> |  <p>图 42. Post Filter FFT and Ripple Under Light Load</p> |
| 3.5 | Full Load |  <p>图 43. DC/DC FFT and Ripple Under Full Load</p> |  <p>图 44. Post Filter FFT and Ripple Under Full Load</p> |
| 5 | Light Load |  <p>图 45. DC/DC FFT and Ripple Under Light Load</p> |  <p>图 46. Post Filter FFT and Ripple Under Light Load</p> |

表 14. 1.35-V Ripple and FFT Plot (continued)

| INPUT VOLTAGE (V) | LOAD CONDITION | PRE FILTER | POST FILTER |
|-------------------|----------------|--|---|
| 5 | Full Load |  <p>图 47. DC/DC FFT and Ripple Under Full Load</p> |  <p>图 48. Post Filter FFT and Ripple Under Full Load</p> |
| 5.5 | Light Load |  <p>图 49. DC/DC FFT and Ripple Under Light Load</p> |  <p>图 50. Post Filter FFT and Ripple Under Light Load</p> |
| 5.5 | Full Load |  <p>图 51. DC/DC FFT and Ripple Under Full Load</p> |  <p>图 52. Post Filter FFT and Ripple Under Full Load</p> |

7.2.4 1.2-V Output

表 15. 1.2-V Ripple and FFT Plot

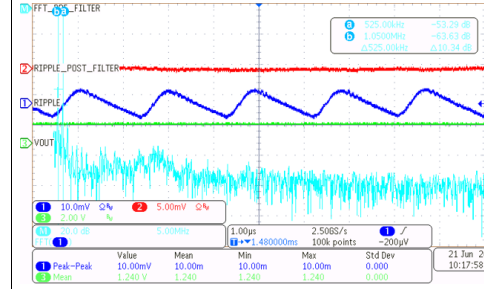
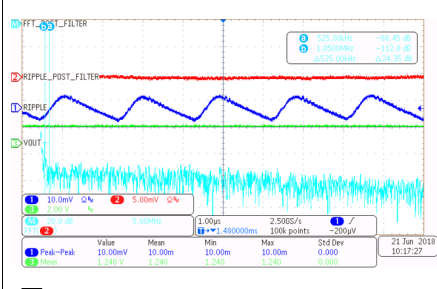
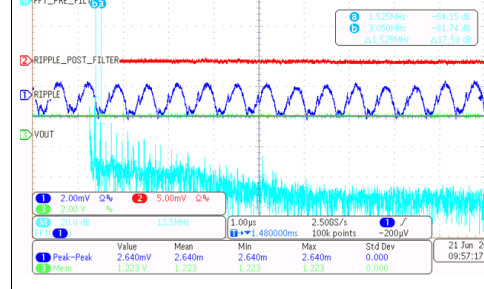
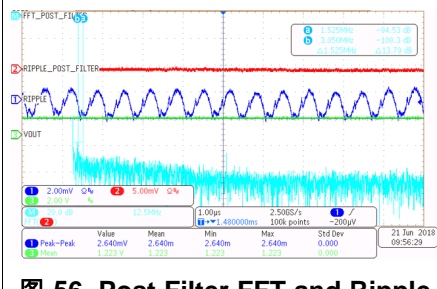
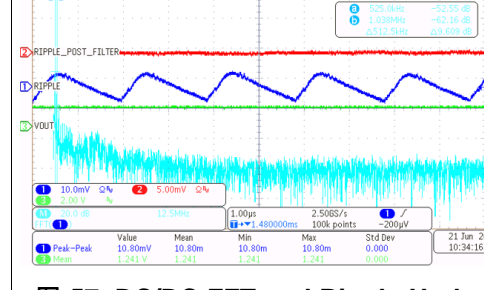
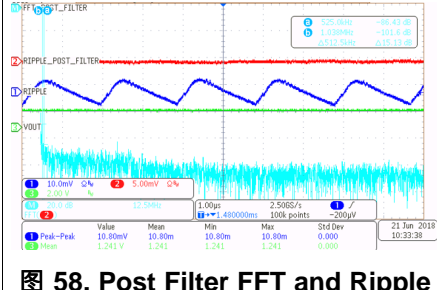
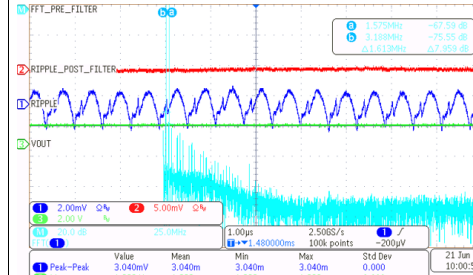
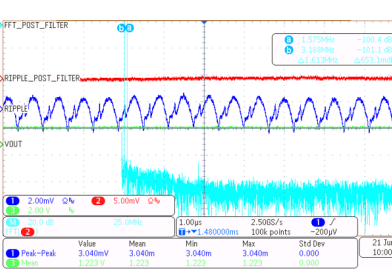
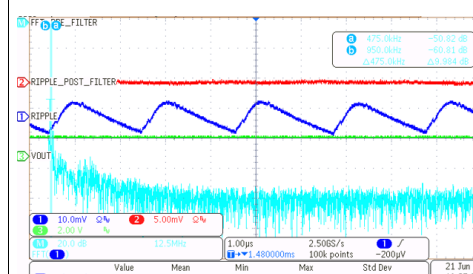
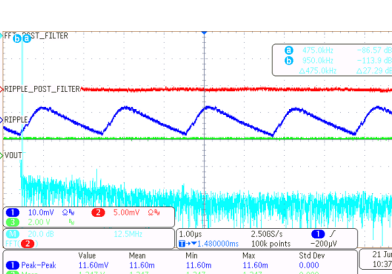
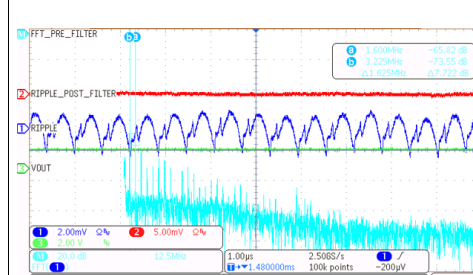
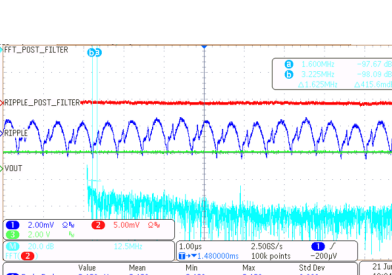
| INPUT VOLTAGE (V) | LOAD CONDITION | PRE FILTER | POST FILTER |
|-------------------|----------------|--|---|
| 3.5 | Light Load |  <p>图 53. DC/DC FFT and Ripple Under Light Load</p> |  <p>图 54. Post Filter FFT and Ripple Under Light Load</p> |
| 3.5 | Full Load |  <p>图 55. DC/DC FFT and Ripple Under Full Load</p> |  <p>图 56. Post Filter FFT and Ripple Under Full Load</p> |
| 5 | Light Load |  <p>图 57. DC/DC FFT and Ripple Under Light Load</p> |  <p>图 58. Post Filter FFT and Ripple Under Light Load</p> |

表 15. 1.2-V Ripple and FFT Plot (continued)

| INPUT VOLTAGE (V) | LOAD CONDITION | PRE FILTER | POST FILTER |
|-------------------|----------------|---|--|
| 5 | Full Load |  <p>图 59. DC/DC FFT and Ripple Under Full Load</p> |  <p>图 60. Post Filter FFT and Ripple Under Full Load</p> |
| 5.5 | Light Load |  <p>图 61. DC/DC FFT and Ripple Under Light Load</p> |  <p>图 62. Post Filter FFT and Ripple Under Light Load</p> |
| 5.5 | Full Load |  <p>图 63. DC/DC FFT and Ripple Under Full Load</p> |  <p>图 64. Post Filter FFT and Ripple Under Full Load</p> |

7.2.5 1.8-V Output

表 16. 1.8-V Ripple and FFT Plot

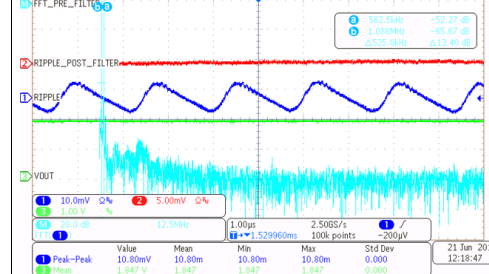
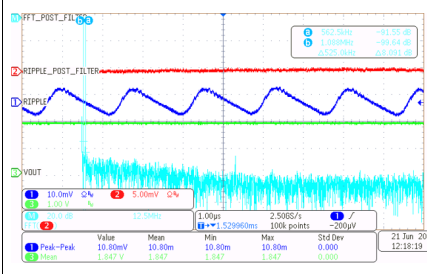
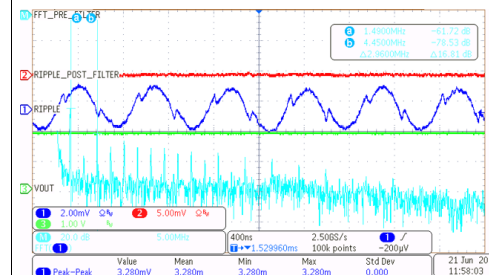
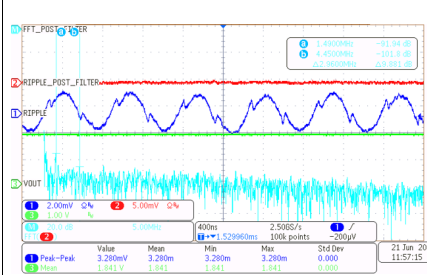
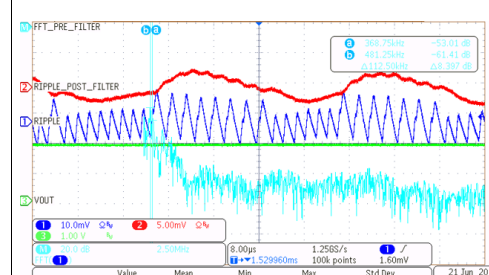
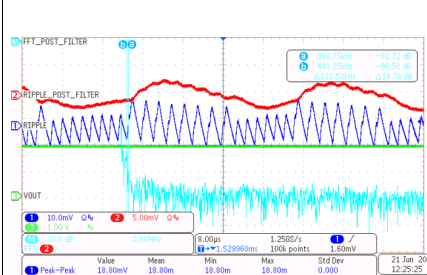
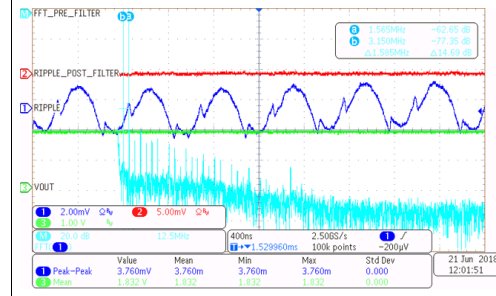
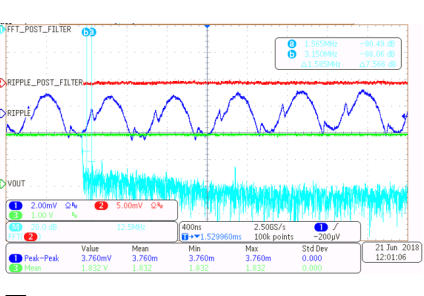
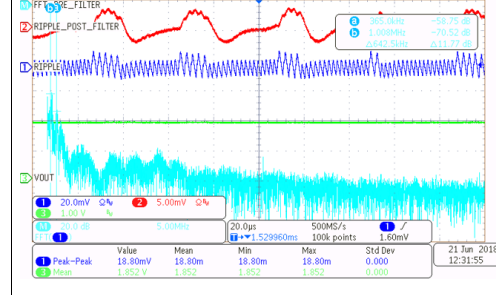
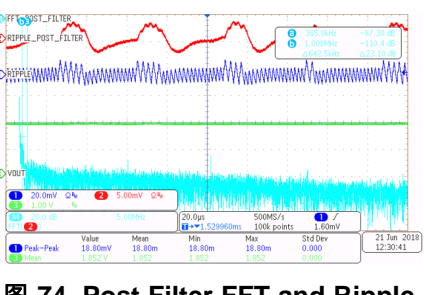
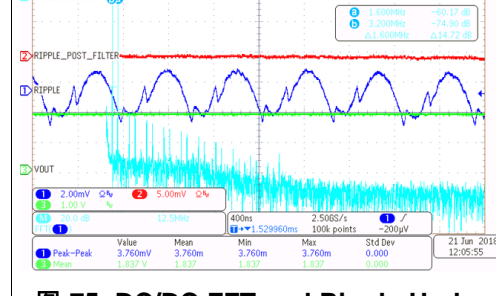
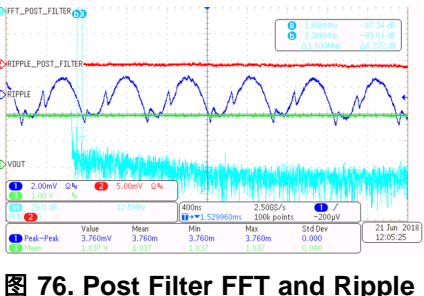
| INPUT VOLTAGE (V) | LOAD CONDITION | PRE FILTER | POST FILTER |
|-------------------|----------------|---|--|
| 3.5 | Light Load |  <p>图 65. DC/DC FFT and Ripple Under Light Load</p> |  <p>图 66. Post Filter FFT and Ripple Under Light Load</p> |
| 3.5 | Full Load |  <p>图 67. DC/DC FFT and Ripple Under Full Load</p> |  <p>图 68. Post Filter FFT and Ripple Under Full Load</p> |
| 5 | Light Load |  <p>图 69. DC/DC FFT and Ripple Under Light Load</p> |  <p>图 70. Post Filter FFT and Ripple Under Light Load</p> |

表 16. 1.8-V Ripple and FFT Plot (continued)

| INPUT VOLTAGE (V) | LOAD CONDITION | PRE FILTER | POST FILTER |
|-------------------|----------------|--|---|
| 5 | Full Load |  <p>图 71. DC/DC FFT and Ripple Under Full Load</p> |  <p>图 72. Post Filter FFT and Ripple Under Full Load</p> |
| 5.5 | Light Load |  <p>图 73. DC/DC FFT and Ripple Under Light Load</p> |  <p>图 74. Post Filter FFT and Ripple Under Light Load</p> |
| 5.5 | Full Load |  <p>图 75. DC/DC FFT and Ripple Under Full Load</p> |  <p>图 76. Post Filter FFT and Ripple Under Full Load</p> |

7.3 Point of Load Transient Response

Each DC/DC rail has been tested for Transient load condition ranging from (50 mA to 1 A/250 mA) using DC electronic load with 10-kHz switching frequency, 50% duty cycle and 250 mA/ μ s slew rate to capture and compare FFT spectrum of DC/DC output rail with Post Filter Response. Also overshoot, undershoot is observed to validate fast transient response. From test result we clearly see ripple voltage changing under load condition and having low and high frequency switching components. Using external filter we can achieve clean DC output immune to switching harmonics across wide load conditions

表 17. Transient Response

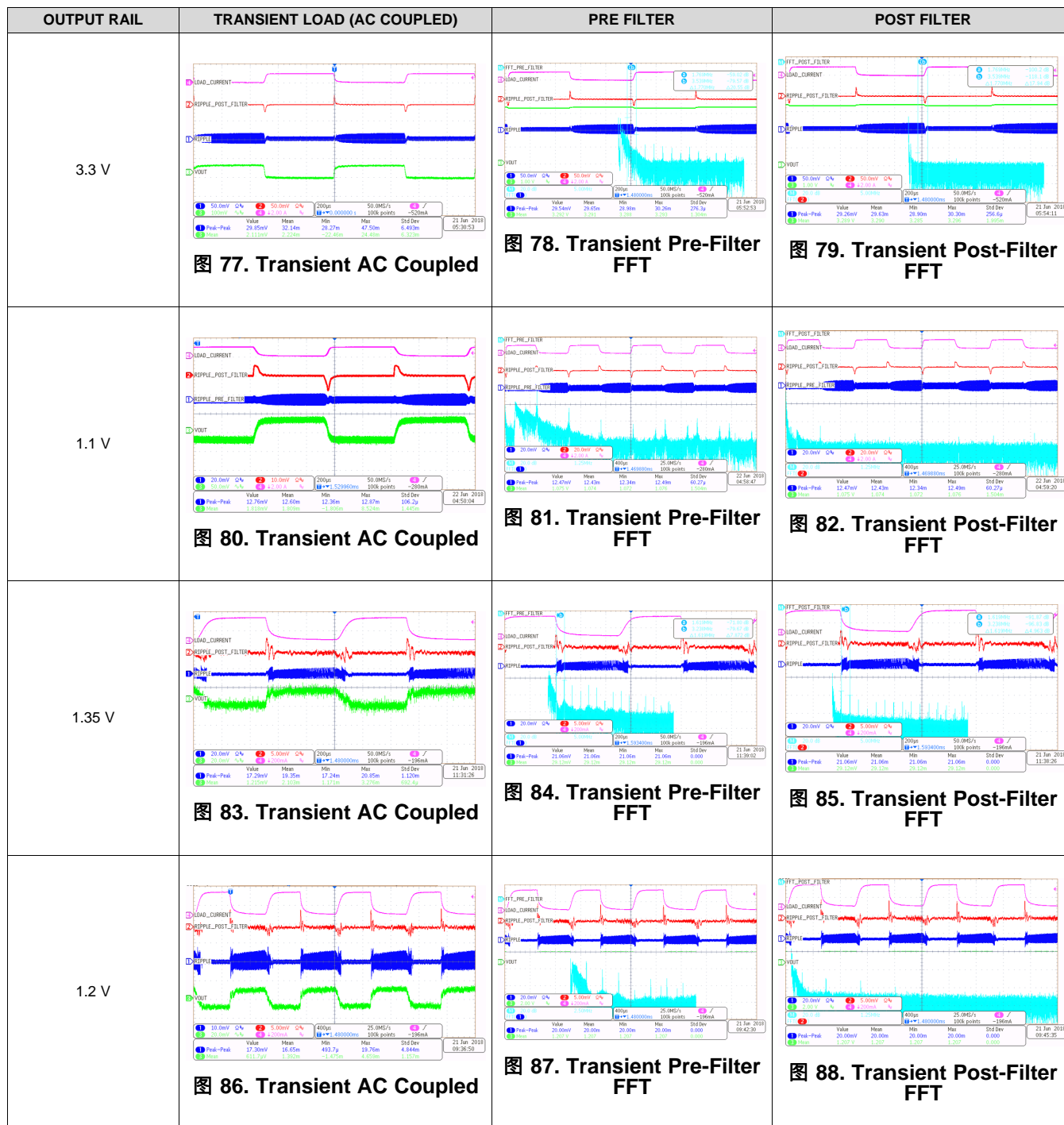
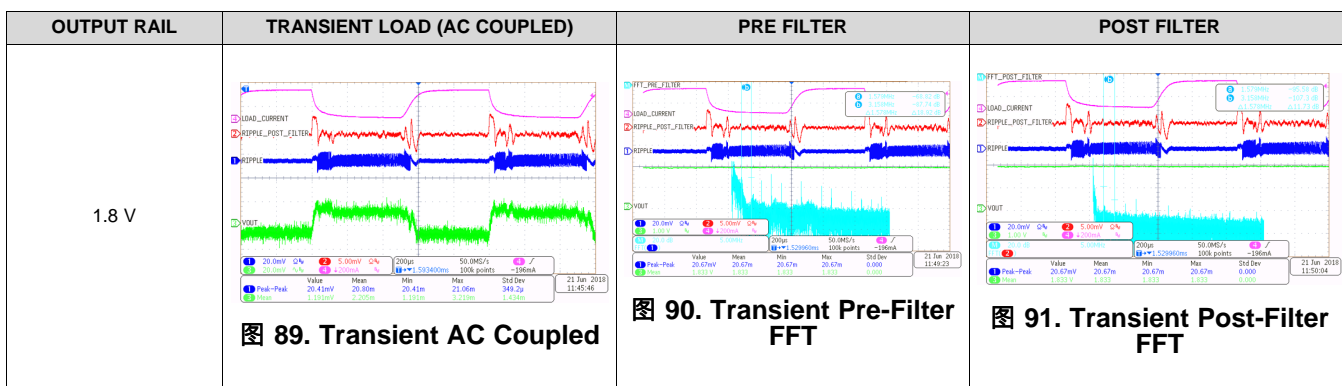


表 17. Transient Response (continued)



7.4 Sequencing

TIDA-01579 Board supports both passive and active sequencing. Resistor divider as shown in schematic can be modified to passive RC circuit to design passive sequencing. Generic passive sequencing has been implemented and tested to meet most common sequencing for Core Voltage (1.1 V), DDR3L Voltage (1.35 V) and 3.3-V rail. Using Port expander and Power Good output of DC/DC digital sequencing is also possible



图 92. Passive Sequencing 0.1 V, 1.35 V, 3.3 V, and 1.8 V

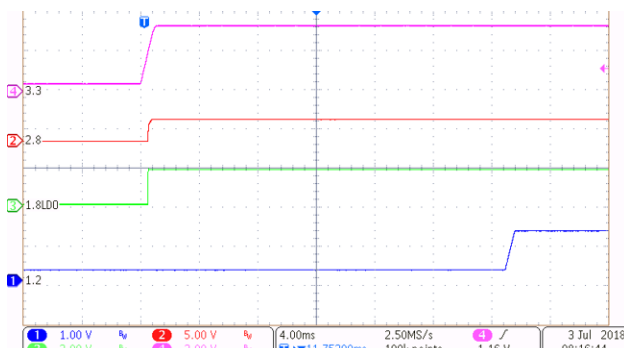


图 93. Passive Sequencing 2.8 V, 1.8 V, and 1.2 V

7.5 Thermal Performance

TIDA-01579 has been targeted to achieve very low thermal dissipation in small form factor. Using IR Thermal Gun at full load condition we see the overall board temperature is below 45°C at room temperature

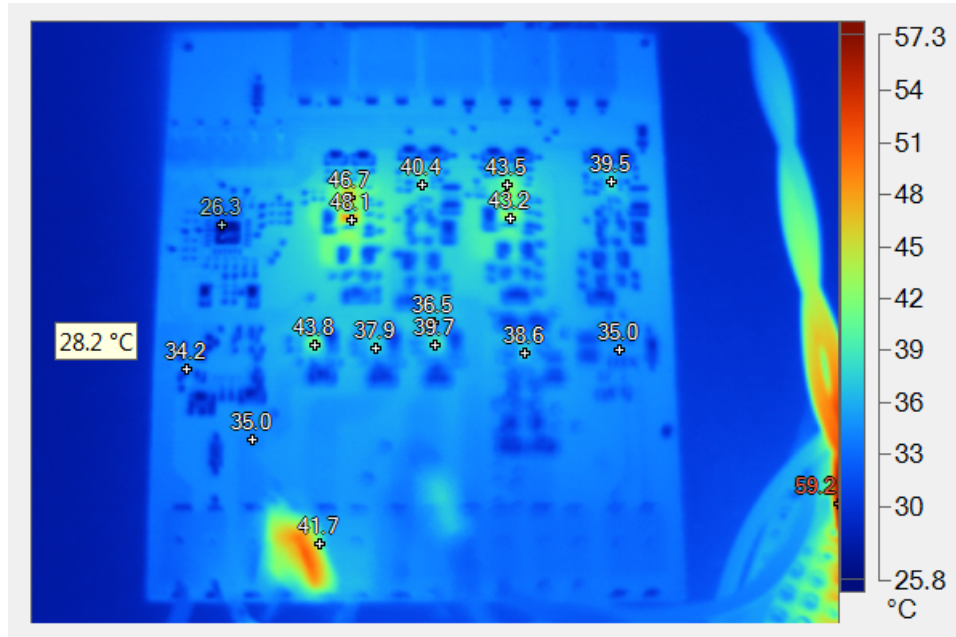


图 94. Thermal Performance

8 Design Files

8.1 Schematics

To download the schematics, see the design files at [TIDA-01579](#).

8.2 Bill of Materials

To download the bill of materials (BOM), see the design files at [TIDA-01579](#).

8.3 PCB Layout Recommendations

8.3.1 Layout Prints

To download the layer plots, see the design files at [TIDA-01579](#).

8.4 Altium Project

To download the Altium Designer® project files, see the design files at [TIDA-01579](#).

8.5 Gerber Files

To download the Gerber files, see the design files at [TIDA-01579](#).

8.6 Assembly Drawings

To download the assembly drawings, see the design files at [TIDA-01579](#).

9 Related Documentation

1. Texas Instruments, [TLV62568 1-A High Efficiency Step-down Converter in SOT23 Package Data Sheet](#)
2. Texas Instruments, [TPS6282x 6-V, 1-,2-,3-A Step-Down Converter with DCS-Control™ Data Sheet](#)
3. Texas Instruments, [TLV742P 200mA, Small-Size, Low-Dropout Linear Voltage Regulator Data Sheet](#)
4. Texas Instruments, [TCA9535 Low Voltage 16-Bit I2C and SMBus Low-Power I/O Expander Data Sheet](#)
5. Texas Instruments, [TPS61169 38-V High Current-Boost WLED Driver with PWM Control Data Sheet](#)
6. Texas Instruments, [TPS22976 5.7-V, 6-A, 14-mΩ On-Resistance Dual-Channel Load Switch Data Sheet](#)

9.1 商标

E2E, DCS-Control are trademarks of Texas Instruments.

Altium Designer is a registered trademark of Altium LLC or its affiliated companies.

Wi-Fi is a registered trademark of Wi-Fi Alliance.

All other trademarks are the property of their respective owners.

10 About the Author

SRINIVASAN IYER is a Systems Architect at Texas Instruments India where he is responsible for developing reference design solutions for the industrial segment. Srinivasan has expertise in power supply and analog circuit for Imaging , Video Processing, High Speed and Motor Control Systems.

重要声明和免责声明

TI 均以“原样”提供技术性及可靠性数据（包括数据表）、设计资源（包括参考设计）、应用或其他设计建议、网络工具、安全信息和其他资源，不保证其中不含任何瑕疵，且不做任何明示或暗示的担保，包括但不限于对适销性、适合某特定用途或不侵犯任何第三方知识产权的暗示担保。

所述资源可供专业开发人员应用TI 产品进行设计使用。您将对以下行为独自承担全部责任：(1) 针对您的应用选择合适的TI 产品；(2) 设计、验证并测试您的应用；(3) 确保您的应用满足相应标准以及任何其他安全、安保或其他要求。所述资源如有变更，恕不另行通知。TI 对您使用所述资源的授权仅限于开发资源所涉及TI 产品的相关应用。除此之外不得复制或展示所述资源，也不提供其它TI 或任何第三方的知识产权授权许可。如因使用所述资源而产生任何索赔、赔偿、成本、损失及债务等，TI 对此概不负责，并且您须赔偿由此对TI 及其代表造成的损害。

TI 所提供产品均受TI 的销售条款 (<http://www.ti.com.cn/zh-cn/legal/termsofsale.html>) 以及ti.com.cn 上或随附TI 产品提供的其他可适用条款的约束。TI 提供所述资源并不扩展或以其他方式更改TI 针对TI 产品所发布的可适用的担保范围或担保免责声明。

邮寄地址：上海市浦东新区世纪大道 1568 号中建大厦 32 楼，邮政编码：200122
Copyright © 2018 德州仪器半导体技术（上海）有限公司

重要声明和免责声明

TI 均以“原样”提供技术性及可靠性数据（包括数据表）、设计资源（包括参考设计）、应用或其他设计建议、网络工具、安全信息和其他资源，不保证其中不含任何瑕疵，且不做任何明示或暗示的担保，包括但不限于对适销性、适合某特定用途或不侵犯任何第三方知识产权的暗示担保。

所述资源可供专业开发人员应用TI 产品进行设计使用。您将对以下行为独自承担全部责任：(1) 针对您的应用选择合适的TI 产品；(2) 设计、验证并测试您的应用；(3) 确保您的应用满足相应标准以及任何其他安全、安保或其他要求。所述资源如有变更，恕不另行通知。TI 对您使用所述资源的授权仅限于开发资源所涉及TI 产品的相关应用。除此之外不得复制或展示所述资源，也不提供其它TI 或任何第三方的知识产权授权许可。如因使用所述资源而产生任何索赔、赔偿、成本、损失及债务等，TI 对此概不负责，并且您须赔偿由此对TI 及其代表造成的损害。

TI 所提供产品均受TI 的销售条款 (<http://www.ti.com.cn/zh-cn/legal/termsofsale.html>) 以及ti.com.cn 上或随附TI 产品提供的其他可适用条款的约束。TI 提供所述资源并不扩展或以其他方式更改TI 针对TI 产品所发布的可适用的担保范围或担保免责声明。

邮寄地址：上海市浦东新区世纪大道 1568 号中建大厦 32 楼，邮政编码：200122
Copyright © 2018 德州仪器半导体技术（上海）有限公司